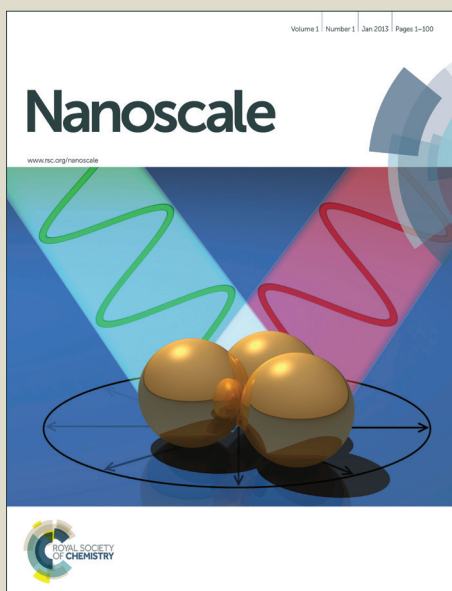


# Nanoscale

Accepted Manuscript



This is an *Accepted Manuscript*, which has been through the Royal Society of Chemistry peer review process and has been accepted for publication.

*Accepted Manuscripts* are published online shortly after acceptance, before technical editing, formatting and proof reading. Using this free service, authors can make their results available to the community, in citable form, before we publish the edited article. We will replace this *Accepted Manuscript* with the edited and formatted *Advance Article* as soon as it is available.

You can find more information about *Accepted Manuscripts* in the [Information for Authors](#).

Please note that technical editing may introduce minor changes to the text and/or graphics, which may alter content. The journal's standard [Terms & Conditions](#) and the [Ethical guidelines](#) still apply. In no event shall the Royal Society of Chemistry be held responsible for any errors or omissions in this *Accepted Manuscript* or any consequences arising from the use of any information it contains.



Journal Name

ARTICLE

## Enhanced ultraviolet-visible light responses of phototransistors based on individual and few ZrS<sub>3</sub> nanobelts

Received 00th January 20xx,  
Accepted 00th January 20xx

You-Rong Tao, Jia-Jing Wu and Xing-Cai Wu\*

DOI: 10.1039/x0xx00000x

Phototransistors based on individual and three ZrS<sub>3</sub> nanobelts were fabricated on SiO<sub>2</sub>/Si wafers by photolithograph and lift-off technique, respectively, and their light-induced electric properties were investigated in detail. Both the devices demonstrate remarkable photoresponse from ultraviolet to near infrared light. Photoswitch current ratio (PCR) of the single-nanobelt phototransistor is 13 under 405-nm light illumination with an optical power of 10.5 mW/cm<sup>2</sup> at a bias of 5 V, while the PCR of the three-nanobelts device is 210 under 405-nm light illumination of 5.57 mW/cm<sup>2</sup> at a bias of 1 V. By comparison of the photoresponses under the same conditions, the latter is superior to the former, and both the devices are much better photoresponse than the reported flexible ZrS<sub>3</sub>-nanobelt-film photodetector.

www.rsc.org/

### Introduction

Over two decades, one-dimensional (1D) nanostructures have attracted great attention due to their unique physical properties and applications in high-performance nanodevices based on their high surface to volume ratios and rationally designed surface.<sup>1–12</sup> For example, individual semiconducting nanowire can be fabricated into field effect transistor (FET), and developed into photodetectors<sup>13</sup> and gas sensors.<sup>14</sup> So far, a few individual 1D nanostructures, such as ZnSe,<sup>15</sup> In<sub>2</sub>Ge<sub>2</sub>O<sub>7</sub>,<sup>16</sup> β-Ga<sub>2</sub>O<sub>3</sub>,<sup>17</sup> and Ta<sub>3</sub>N<sub>5</sub> nanobelt,<sup>18</sup> ZnS/ZnO biaxial nanobelt,<sup>19</sup> ZnO-SnO<sub>2</sub> heterojunction nanofibers,<sup>20</sup> GaAs/AlGaAs core-shell nanowire,<sup>21</sup> WS<sub>2</sub> nanotube<sup>22</sup> and so on, have been fabricated into photodetectors. On the basis of the design idea, Li et al. once constructed an individual ZrS<sub>2</sub> nanobelt phototransistor and found its excellent visible-light response.<sup>23</sup> ZrS<sub>2</sub> is one of layered transition metal dichalcogenides (TMDs) which contains metal layer sandwiched between two chalcogen layers with the metal in an octahedral coordination model.<sup>24</sup> The ZrS<sub>2</sub> nanobelts were synthesized by a vacuum prolysis of ZrS<sub>3</sub> nanobelts.<sup>25</sup> Subsequently, we found the broad visible-light responses of transition metal trichalcogenides (TMTs) such as ZrS<sub>3</sub>,<sup>26</sup> HfS<sub>3</sub>,<sup>27</sup> ZrSe<sub>3</sub> and HfSe<sub>3</sub>.<sup>28</sup> TMTs are another type of layered compounds which are composed of MX<sub>3</sub> (M: IV–VIB metals; X: S, Se and Te). Their crystals process a pseudo 1D structure where there is an infinite chain of trigonal prismatic (MX<sub>6</sub>) units extending parallel to the b-axis and sharing upper and lower faces. The chains with strong ionic covalent (or metallic) bond are separated by a relatively large distance and interchain bond.<sup>29</sup> ZrS<sub>3</sub> is a p-type semiconductor which room-temperature resistivity is 15 Ωcm, and possesses a direct optical band gap of 2.56 eV at room temperature and two indirect optical band gaps of 2.055 eV (E//b) and 2.058 eV (E⊥b)

at liquid helium temperature.<sup>29</sup> We once fabricated ZrS<sub>3</sub>-nanobelt film onto polypropylene substrate as a flexible photodetector, and discovered its good photoresponses ranging from 350 to 780 nm. The light on/off current ratio was about 3.5 at a bias of 5 V under illumination of 405-nm light of 12.1 mW/cm<sup>2</sup> with a photoswitch period of 50 s.<sup>26</sup> ZrS<sub>3</sub> is a broad photoresponse material from ultraviolet (UV) to near-infrared (NIR), and low-cost, however so far, many photosensitive materials are still limited to separate photosensitive region, so it is an important actual meaning to make a new broad and high-photosensitive ZrS<sub>3</sub>-based photodetector. Here we fabricated individual and three ZrS<sub>3</sub> nanobelts onto SiO<sub>2</sub>/Si substrates to form field effect transistors, respectively, and found their enhancements of the broad visible-light responses. Specially, the photoswitch current ratio (PCR) of the three-nanobelt phototransistor is 210 under 405-nm light illumination of 5.57 mW/cm<sup>2</sup> at a bias of 1 V, much greater than that (3.5) of the reported ZrS<sub>3</sub> flexible photodetector. It is a great progress, so we report the results.

### Experimental method

#### Synthetic procedures and characterization

The ZrS<sub>3</sub> nanobelts may be synthesized by a chemical vapor transportation (CVT) of sulfur and zirconium (Zr) plates,<sup>25</sup> or Zr powders.<sup>30, 31</sup> Here the latter method was selected. In a typical process, Zr powders (100.0 mg; Zr ≥ 99.95%) and sulfur powders (105.4 mg; S ≥ 99.5%) with an atomic ratio of 1: 3 were sealed in a quartz ampoule under vacuum (Φ6 mm × 12 cm, ca. 10<sup>-2</sup> Pa). The quartz ampoule was then placed in a conventional horizontal furnace with a temperature gradient of ca. 10 Kcm<sup>-1</sup> from centre to edge along axial direction, and the end with the mixture powders were put at the centre of the furnace. In the following, the furnace was heated to 650 °C and maintained at the temperature for 10 h. Finally, the reagents were completely converted into ZrS<sub>3</sub> nanobelts. The as-prepared ZrS<sub>3</sub> nanobelts were characterized by X-ray diffraction (XRD, Shimadzu XRD-6000 with graphite monochromatized Cu K<sub>α1</sub> radiation), a field-emission scanning electron microscope (FE-

School of Chemistry and Chemical Engineering, Key Laboratory of Mesoscopic Chemistry of MOE, Nanjing University, Nanjing, 210093, P. R. China. E-mail: [wuxingqca@nju.edu.cn](mailto:wuxingqca@nju.edu.cn); Fax: 86-25-83317761.

† Footnotes relating to the title and/or authors should appear here. Electronic Supplementary Information (ESI) available: [details of any supplementary information available should be included here]. See DOI: 10.1039/x0xx00000x

SEM, Hitachi S-4800), and a high-resolution transmission electron microscope (HRTEM, JEM-2100). Ultraviolet-visible (UV-vis.) absorbance spectrum was recorded by a Shimadzu UV-3600 spectrophotometer.

### Device measurements

The current–voltage ( $I$ - $V$ ) and the current–time ( $I$ - $t$ ) characteristics were measured by Model CRX-4K Cryogenic Probe Station (Lake Shore Inc.) and Keithley 2636 source meter (Keithley Instruments Inc.) The spectral response was recorded under illumination of different wavelength laser. A spectroscopic response ranging from 350 to 1000 nm was measured using a 300 W Xenon lamp (HSX-UV300), and a multi-grating monochromator (71SW151) with order sorting filters was used. Wavelength was controlled and adjusted by applied software. Optical intensity was adjusted by applying currents and an aperture. Optical power was measured with FZ-A radiometer (made in Beijing Normal University). Ultraviolet (UV) optical power was measured with UV light radiometer UV340B (made in China). The experiments have been done at room temperature in air except specially proposing condition.

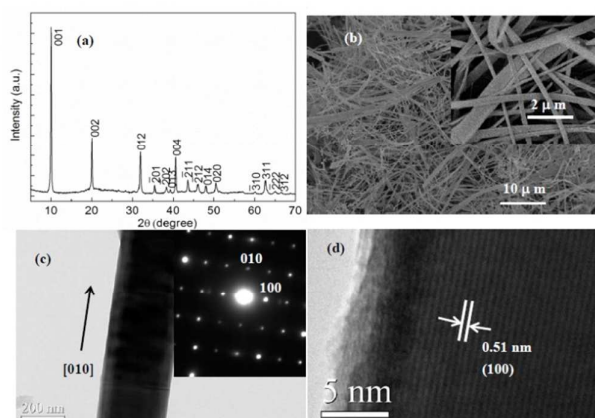


**Fig. 1** (a) XRD pattern and (b) low-magnification SEM image of  $ZrS_3$  nanobelts; inset shows high-magnification image. (c) TEM image of a single  $ZrS_3$  nanobelt. Inset shows its SAED pattern. (d) HRTEM image of individual  $ZrS_3$  nanobelt corresponding to (c).

## Results and discussion

An X-ray diffraction (XRD) pattern of the as-prepared nanobelts is shown in Fig. 1a. All the diffraction peaks can be readily indexed to a monoclinic  $ZrS_3$  phase (PCPDFWIN 30-1498;  $a=0.5124$  nm,  $b=0.3624$  nm,  $c=0.898$  nm, and  $\beta=97.28^\circ$ ), so they are pure phase. Here the XRD pattern is that of  $ZrS_3$  nanobelt powders, so it is different from that of  $ZrS_3$  nanobelt arrays on a Zr substrate in Ref. 26, which is attributed to the different orientation of the materials in the process of measurement, but both can be indexed as the same  $ZrS_3$  phase.

The field-emission scanning electron microscopy (SEM) recorded their morphologies. Fig. 1b is a SEM image of the nanobelts, revealing that the products are a high-yield nanobelt with a width of about 30 to 500 nm, a thickness of about 10 to 30 nm, and

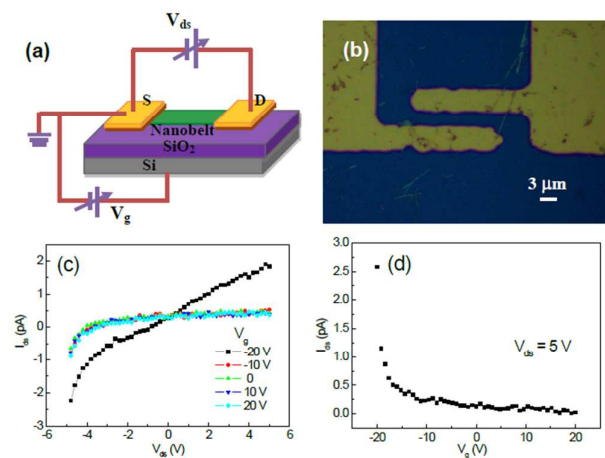


**Fig. 2** (a) Schematic illustration of  $ZrS_3$  nanowire field effect transistor (FET). (b) Optical micrograph of the FET device of individual  $ZrS_3$  nanobelt (device 1). (c) Plots of drain current ( $I_{ds}$ ) vs. voltage ( $V_{ds}$ ) at different gate voltage. (d) Electrical characteristic of the device 1 at  $V_{ds}=5V$ .

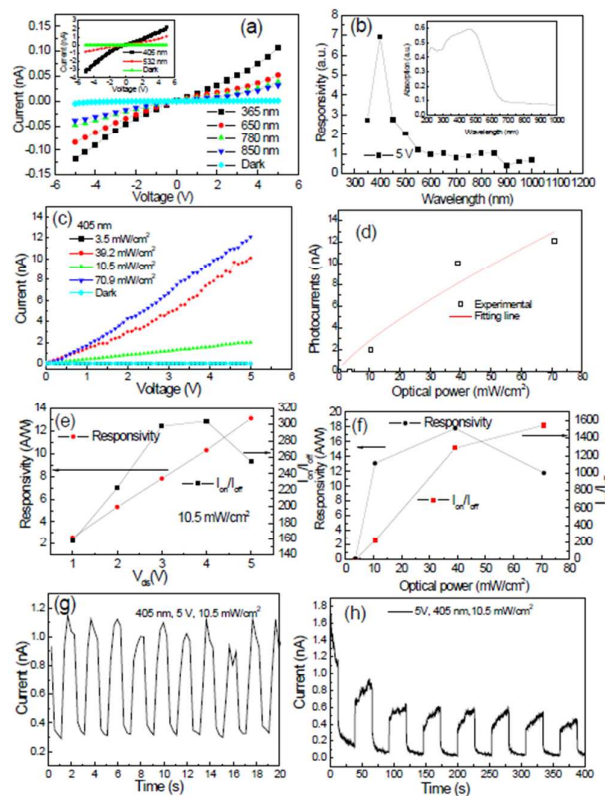


**Fig. 3** (a)  $I$ - $V$  curves of device 1 under different-wavelength light illumination, and in dark. (b) Responsivity of device 1 at a bias of 5 V to wavelengths from 350 to 1000 nm. Inset: UV-vis absorbance spectrum of  $ZrS_3$  nanobelts. (c)  $I$ - $V$  and (d) photocurrent–optical power curves of the device 1 under illumination of 405-nm light with different optical powers. (e) Dependence of responsivity and  $I_{on}/I_{off}$  on  $V_{gs}$  under 405 nm-light illumination of  $10.5 \text{ mW/cm}^2$ . (f) Dependence of responsivity and  $I_{on}/I_{off}$  on optical powers. (g) and (h)  $I$ - $t$  characteristics of the device 1 under illumination of 405-nm light with a photoswitch period of 1 and 25 s, respectively.

a length up to 20  $\mu\text{m}$ . Fig. 1c exhibits a transmission electron microscopy (TEM) image of individual  $\text{ZrS}_3$  nanobelt, and inset shows corresponding selected area electron diffraction (SAED) pattern on the upper right corner, and confirming that the nanobelt grew along [010] direction. Fig. 1d reveals high-resolution TEM (HRTEM) image of the individual nanobelt in Fig. 1c. Lattice fringe spacing of 0.51 nm coincides with d-values of (100) plane of above monoclinic  $\text{ZrS}_3$  phase.

Fig. 2a represents a schematic illustration of  $\text{ZrS}_3$ -nanobelt FETs, while Fig. 2b shows a micrograph of the FET, namely, the nanobelts were put in ethanol and dispersed by ultrasonic for a few minutes, and then were transferred onto the surface of  $\text{SiO}_2/\text{Si}$ , and then two Ti/Au (10 nm/100 nm) electrodes were deposited on both ends of the nanobelts by photolithography and lift-off technique. Fig. 2c exhibits the transfer characteristic of the FET of the individual nanobelt at a bias of 5 V. It can be seen that the conductance of the nanobelts decreases as the gate voltages rise, suggesting that the nanobelts are p-type semiconductors. A linear-region transconductance  $g_m$  ( $dI_{\text{sd}}/dV_g$ ) is  $-1.1 \times 10^{-12}$  A/V. Electronic mobility ( $\mu$ ) can be calculated from the equation:  $\mu = g_m W / (C_0 V_{\text{sd}} L)$ , where  $W$  and  $L$  are channel width and length, respectively.  $C_0$  is the gate capacitance which is equal to  $\epsilon_r \epsilon_0 / d$ , where  $\epsilon$  is the dielectric constant ( $\epsilon_r = 3.9$  for  $\text{SiO}_2$ ),  $W$  and  $L$  are 0.3 and 4.8  $\mu\text{m}$ , respectively, and  $d$  is the thickness (300 nm) of the gate oxide layer. From the above equation, the mobility of the nanobelt is about  $1.2 \times 10^{-6}$   $\text{cm}^2 \text{V}^{-1} \text{s}^{-1}$ , lower than that of the reported  $\text{ZrS}_2$  nanobelt.<sup>23</sup>

To measure photosensitivity of the device, a monochromatic light was vertically illuminated and the corresponding current–voltage curves were recorded. Fig. 3a displays the  $I$ – $V$  curves of device 1 (Fig. 2b) at  $V_g = 0$  V under light illumination and in the dark. The nonlinearity and asymmetry of the curves indicate non ohmic contact between the Ti/Au electrodes and the nanobelts. Compared with the dark state, the currents increase under light illumination at the same bias voltage, which reveals the photosensitivity of the device from ultraviolet light (365 nm) to near infrared (NIR) (850 nm). As illustrated in Fig. 3b, responsivity ( $R_x$ ) of device 1 to light wavelength<sup>20</sup> reveals that the cut-off wavelength is about 900 nm and optimal photosensitivity should be the region from ultraviolet to visible light, similar to the UV-vis absorbance spectrum of the  $\text{ZrS}_3$  nanobelts (inset). Here absorbance edge of  $\text{ZrS}_3$  nanobelts is not equal to cut-off wavelength. The phenomenon can be also observed in other literature,<sup>32</sup> so absorbance edge is not able to take place of cut-off wavelength. Fig. 3c exhibits the  $I$ – $V$  curves of the device 1 illuminated by 405-nm light of various optical powers, showing that the device is sensitive to light strength, and the corresponding photocurrent–optical power curve is plotted in Fig. 3d at a bias of 5 V, which can be fitted with a power law of  $I_p = \alpha P^\theta$ , where  $I_p$  is photocurrent (nA) which is the difference between the currents under light illumination and in the dark, where  $\alpha$  is coefficient,  $\theta$  is exponent, and  $P$  is an optical power ( $\text{mW}/\text{cm}^2$ ). The fitting gives  $I_p = 0.45 P^{0.79}$ . The non-unity exponent is a result of the complex process of electron-hole generation, trapping, and recombination in the semiconductor.<sup>33</sup> It clearly indicates the high selectivity and sensitivity of the photodetector. On the basis of Fig. 3c, dependence of responsivity and PCR ( $I_{\text{on}}/I_{\text{off}}$ ) on  $V_{\text{ds}}$  at an optical power of 10.5  $\text{mW}/\text{cm}^2$  is plotted in Fig. 3e. With the increase of  $V_{\text{ds}}$ , the responsivity linearly increases, and after  $I_{\text{on}}/I_{\text{off}}$  increases to maximum at  $V_{\text{ds}} = 4$  V, it starts to decrease. Fig. 3f displays dependence of responsivity and  $I_{\text{on}}/I_{\text{off}}$  on optical power at  $V_{\text{ds}} = 5$  V. As optical powers increase,  $I_{\text{on}}/I_{\text{off}}$  increases, and after responsivity reaches a maximum at an optical power of 40  $\text{mW}/\text{cm}^2$ , it starts to decrease. So responsivity and  $I_{\text{on}}/I_{\text{off}}$  depend on  $V_{\text{ds}}$  and optical powers. Low  $V_{\text{ds}}$  and optical power, and high  $I_{\text{on}}/I_{\text{off}}$  are important quota of photodetector. Fig. 3g shows the time-dependent current of the device 1 at a bias of 5 V under 450-nm light illumination of 10.5

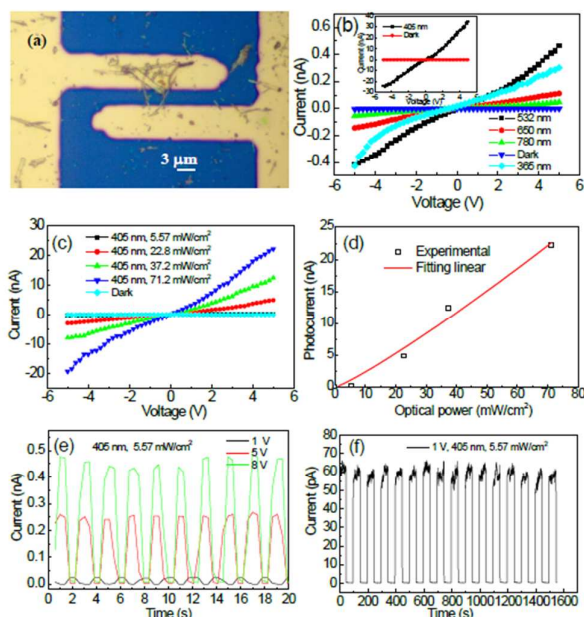


**Fig. 4** (a) Micrograph of three  $\text{ZrS}_3$  nanobelt photodetector (device 2). (b)  $I$ – $V$  curves of device 2 under illumination of different wavelength light, and under dark condition. (c)  $I$ – $V$  and (d) photocurrent–optical power curves of the device 2 under illumination of 405-nm light with different optical powers. (e) and (f) Time-dependent responses of device 2 at a bias of 1 V under illumination of 405-nm light with photoswitch period of 1 and 50 s.

$\text{mW}/\text{cm}^2$  with a photoswitch period of 1 s. The PCR is 3.4, and the responsivity is 1.8 A/W, and the response time (rise time/decay time) is 0.4/0.33 s. The time taken for the current to increase from 10% to 90% of the peak value or vice versa is defined as the rise time and decay time, respectively. Fig. 3h reveals the time-dependent current of the device 1 under the same condition with a photoswitch period of 25 s, showing photosensitive stability of the device. Here PCR is 13, and response time is below 0.4 s. Because the increase and decay of photocurrent need enough time,<sup>34</sup> different photoswitch period results in different PCR and response time. Here  $R_{405 \text{ nm}} = 3.9$  A/W for Fig. 3h, and the corresponding quantum efficiency (QE) is  $1.1 \times 10^3\%$ .

To compare with individual nanobelt device, the phototransistor based on three  $\text{ZrS}_3$  nanobelts was fabricated, as shown in Fig. 4a (device 2).  $I$ – $V$  curves of device 2 under light illumination and in the dark are shown in Fig. 4b, also confirming excellent photosensitivity of the device from UV-vis to NIR. Fig. 4c reveals  $I$ – $V$  curves of device 2 under illumination of 405-nm light with different optical power and in the dark, and the corresponding photocurrent–optical power characteristic is plotted in Fig. 4d. The curve can be fitted with a power law of  $I_p = 0.126 P^{1.14}$ , where units of  $I_p$  and  $P$  are nA and  $\text{mW}/\text{cm}^2$ , respectively. Fig. 4e shows  $I$ – $t$  curves of device 2 at different bias voltages under the alternative dark and illumination conditions with a photoswitch period of 1 s. The  $I_{\text{on}}/I_{\text{off}}$  are 65, 71 and 64, and the responsivities are 0.13, 1.46, 2.48 A/W at bias of 1, 5 and 8 V, respectively, and all the response time is below 0.4 s. Therefore, as the bias voltages increase, the responsivities increase, but the PCR almost does not change. Fig. 4f is a current dependence on time under the same light illumination condition with a photoswitch period of 50 s at a bias of 1 V, which reveals the photoresponse stability of device 2, too. Here the  $I_{\text{on}}/I_{\text{off}}$  is 210, the response time is below 0.4 s,  $R_{405 \text{ nm}} = 0.36$  A/W, and the corresponding QE is 99%. On the basis of Fig. 3(g) and Fig. 4(e), the

$I_{on}/I_{off}$  (3.4) of device 1 is lower than that (71) of device 2 at the same are adsorbed on the nanobelts surface and capture free electrons

**Table 1** A Comparison of single and three ZrS<sub>3</sub> nanobelt photodetectors with other photodetectors

Photodetectors	Wavelength/power	Bias voltage (V)	$R_{\lambda}$ (A/W)	$I_{on}/I_{off}$	Rise time/decay time (s)	Ref.
CdTe nanoribbon	400 nm/637 $\mu\text{Wcm}^{-2}$	5	12	1.1	~1.1s/~3.3s	35
Zn <sub>3</sub> P <sub>2</sub> nanowire film	620 nm/0.7 mWcm <sup>-2</sup>	2	600	6.3		36
Single-layer MoS <sub>2</sub>	550 nm/80 $\mu\text{W}$	1	$4.2 \times 10^{-4}$		<0.05s	37
H <sub>2</sub> -annealing MoO <sub>3</sub> nanobelt	420 nm/5.6 mWcm <sup>-2</sup>	0.1	55.5			38
ZrS <sub>3</sub> nanobelt film	405nm/12.1 mWcm <sup>-2</sup>	5		3.5	13/28 s	26
GaS nanobelt ( on SiO <sub>2</sub> /Si)	490 nm/0.5 mWcm <sup>-2</sup>	2	$2.3 \times 10^{-3}$			39
$\gamma$ -Ga <sub>2</sub> O <sub>3</sub> nanoflowers	254 nm/6 W	0.5		220		41
Single ZrS <sub>3</sub> nanobelt	405nm/10.5 mWcm <sup>-2</sup>	5	3.9	13	<0.4s	This work
Three ZrS <sub>3</sub> nanobelts	405 nm/5.57 mWcm <sup>-2</sup>	1	0.36	210	<0.4s	This work

bias voltage of 5 V, and they have the same response time (~0.4 s), furthermore, the light-illuminated power (10.5 mW/cm<sup>2</sup>) of device 1 is higher than that (5.57 mW/cm<sup>2</sup>) of device 2, so device 2 is higher photoresponse than device 1 under the same condition. Because the  $I_{on}/I_{off}$  of the flexible ZrS<sub>3</sub>-nanobelt-film photodetector is 1.71 at a bias voltage of 5 V under 405-nm-light illumination with an optical power of 45 mW/cm<sup>2</sup>,<sup>26</sup> device 1 and 2 are both superior to the reported flexible ZrS<sub>3</sub>-nanobelt-film photodetector. Responsivities and  $I_{on}/I_{off}$  of the ZrS<sub>3</sub> nanobelt photodetectors and other photodetectors are included in table 1. The responsivities of the ZrS<sub>3</sub> nanobelt phototransistors are lower than those of the CdTe, Zn<sub>3</sub>P<sub>2</sub> and H<sub>2</sub>-annealing MoO<sub>3</sub> nanobelt photodetectors, but are much higher than those of the GaS nanobelt and single-layer MoS<sub>2</sub>

from the nanobelts (forming O<sub>2</sub><sup>-</sup>), helpful to increase the hole concentration so that conductivity increases because ZrS<sub>3</sub> is a p-type semiconductor. It is different from the photocurrent-enhanced mechanism of the reported ZrS<sub>3</sub> nanobelt-film photodetectors,<sup>26</sup> because both the nanobelts were prepared under different conditions, the former depended on reaction of Zr plates and sulfur powders to grow in rich sulfur easily to form n-type semiconductor, whereas the latter depended on reaction of Zr powders and sulfur powders easily to form p-type semiconductor because of lack of sulfur. Certainly, it will be further studied.

## Conclusions

In summary, we have developed two phototransistors based on individual and three ZrS<sub>3</sub> nanobelts. An investigation into individual nanobelt transistor shows that the ZrS<sub>3</sub> nanobelt is a p-type semiconductor with a mobility of about  $1.2 \times 10^{-6}$  cm<sup>2</sup>V<sup>-1</sup>s<sup>-1</sup>. Both the devices show wide-range and fast-speed photoresponse for UV to NIR light. The PCR of the single-nanobelt-based photodetector is 13 under 405-nm light illumination of 10.5 mW/cm<sup>2</sup> at a bias of 5 V, much less than that (210) of the three-nanobelt-based photodetector under 405-nm light illumination of 5.57 mW/cm<sup>2</sup> at a bias of 1 V. Because the PCR almost does not change as bias voltage changes under the same work condition, the three-nanobelts-based photodetector is higher photoresponse than the single-nanobelt-based.

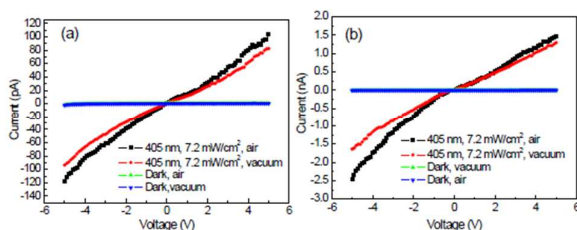


**Fig. 5** The  $I$ - $V$  curves of (a) device 1 and (b) device 2 under a 405-nm light illumination and in the dark in air and vacuum (2.0 Pa).

photodetectors, and both the ZrS<sub>3</sub> phototransistors have high  $I_{on}/I_{off}$ , so they are still excellent photodetectors. Recently,  $\gamma$ -Ga<sub>2</sub>O<sub>3</sub> nanocrystals in glass are reported to become UV-to-visible solar-blind converter and UV emitter.<sup>40</sup> Specially,  $\gamma$ -Ga<sub>2</sub>O<sub>3</sub> nanoflowers have been fabricated to three-electrode-cell-type photodetector and obtained UV PCR of 220 at a bias voltage of 0.5 V.<sup>40</sup> So the ZrS<sub>3</sub> nanobelts may find new applications in photoelectrode and optical glass.

To understand effect of ambience on photosensitivity of the device, the responses of the device 1 and 2 in air and vacuum (2.0 Pa) were investigated. As illustrated in Fig. 5a and b, under dark, the currents of the device 1 are 0.58 and 0.72 pA in vacuum and air at a bias of 5 V, respectively, whereas the currents of the device 2 are 1.48 and 1.32 pA, respectively. The change is no law, so the deviation could originate from error of the meter. Under the 405 nm light illumination, the currents of the device 1 are 82.5 and 104 pA in vacuum and air, respectively, and the currents of the device 2 are 1.29 and 1.48 nA, respectively. Here the current in air is slightly greater than that in vacuum. It can be attributed to effect of oxygen chemisorption/desorption on conductivity. In air, oxygen molecules

## Acknowledgements

This work was supported by the National Science Foundations of China (No. 21171091 and 20671050).

## Notes and references

- Y. N. Xia, P. D. Yang, Y. G. Sun, Y. Y. Wu, B. Mayers, B. Gates, Y. D. Yin, F. Kim and Y. Q. Yan, *Adv. Mater.*, 2003, **15**, 353.
- Y. Huang, X. F. Duan and C. M. Lieber, *Samll.* 2005, **1**, 142.
- C. Yang, C. J. Barrelet, F. Capasso and C. M. Lieber, *Nano Lett.*, 2006, **6**, 2929.
- K. H. Liu, P. Gao, Z. Xu, X. D. Bai and E. G. Wang, *Appl. Phys. Lett.*, 2008, **92**, 213105.
- C. W. Cheng, B. Liu, H. Y. Yang, W. W. Zhou, L. Sun, R. Chen, S. F. Yu, J. X. Zhang, H. Gong, H. D. Sun and H. J. Song, *ACS Nano*, 2009, **3**, 3069.

- 6 G. Z. Shen, D. Chen, P. C. Chen and C. W. Zhou, *ACS Nano*, 2009, **3**, 1115.
- 7 X. S. Fang, Y. Bando, U. K. Gautam, T. Y. Zhai, H. B. Zeng, X. J. Xu, M. Y. Liao and D. Golberg, *Crit. Rev. Solid State Mater. Sci.* 2009, **34**, 190.
- 8 X. C. Wu, Y. R. Tao, Q. X. Gao and Y. L. Zhang, *J. Mater. Chem.*, 2009, **19**, 3883.
- 9 X. C. Wu, J. M. Hong, Y. R. Tao, Y. Deng and Q. X. Gao, *J. Nanosci. Nanotechnol.*, 2010, **10**, 6465.
- 10 X. C. Wu, Y. R. Tao, L. Li, T. Y. Zhai, Y. Bando and D. Golberg, *J. Nanosci. Nanotechnol.* 2011, **11**, 10123.
- 11 Y. Liu, Q. Yang, Y. Zhang, Z. Y. Yang and Z. L. Wang, *Adv. Mater.*, 2012, **24**, 1410.
- 12 F. Zhang, Y. Ding, Y. Zhang, X. L. Zhang and Z. L. Wang, *ACS Nano*, 2012, **6**, 9229.
- 13 H. Kind, H. Q. Yan, B. Messer, M. Law and P. D. Yang, *Adv. Mater.*, 2002, **14**, 158.
- 14 Q. Kuang, C. S. Lao, Z. L. Wang, Z. X. Xie and L. S. Zheng, *J. Am. Chem. Soc.*, 2007, **129**, 6070.
- 15 X. S. Fang, S. L. Xiong, T. Y. Zhai, Y. Bando, M. Y. Liao, U. K. Gautam, Y. Koide, X. G. Zhang, Y. T. Qian and D. Golberg, *Adv. Mater.*, 2009, **21**, 5016.
- 16 L. Li, P. S. Lee, C. Y. Yan, T. Y. Zhai, X. S. Fang, M. Y. Liao, Y. Koide, Y. Bando and D. Golberg, *Adv. Mater.* 2010, **22**, 5145.
- 17 L. Li, E. Auer, M. Y. Liao, X. S. Fang, T. Y. Zhai, U. K. Gautam, A. Lugstein, Y. Koide, Y. Bando and D. Golberg, *Nanoscale* 2011, **3**, 1120.
- 18 X. C. Wu, Y. R. Tao, L. Li, Y. Bando and D. Golberg, *Nanotechnol.*, 2013, **24**, 175701.
- 19 L. F. Hu, J. Yan, M. Y. Liao, H. J. Xiang, X. G. Gong, L. D. Zhang and X. S. Fang, *Adv. Mater.*, 2012, **24**, 2305.
- 20 W. Tian, T. Y. Zhai, C. Zhang, S. L. Li, X. Wang, F. Liu, D. Q. Liu, X. K. Cai, K. Tsukagoshi and D. Golberg, *Adv. Mater.*, 2013, **25**, 4625.
- 21 E. M. Gallo, G. Chen, M. Currie, T. McGuckin, P. Prete, N. Lovergine, B. Nabet and J. E. Spanier, *Appl. Phys. Lett.*, 2011, **98**, 241113.
- 22 C. Y. Zhang, S. Wang, L. J. Yang, Y. Liu, T. T. Xu, Z. Y. Ning, A. Zak, Z. Y. Zhang, R. Tenne and Q. Chen, *Appl. Phys. Lett.*, 2012, **100**, 243101.
- 23 L. Li, X. S. Fang, T. Y. Zhai, M. Y. Liao, U. K. Gautam, X. C. Wu, Y. Koide, Y. Bando and D. Golberg, *Adv. Mater.*, 2010, **22**, 4151.
- 24 C. N. R. Rao and M. Nath, *Dalton Trans.*, 2003, 1.
- 25 Y. L. Zhang, X. C. Wu, Y. R. Tao, C. J. Mao and J. J. Zhu, *Chem. Commun.* 2008, 26832.
- 26 Y. R. Tao, X. C. Wu and W. W. Xiong, *Small*, 2014, **10**, 4905.
- 27 W. W. Xiong, J. Q. Chen, X. C. Wu and J. J. Zhu, *J. Mater. Chem. C*, 2014, **2**, 7392.
- 28 W. W. Xiong, J. Q. Chen, X. C. Wu and J. J. Zhu, *J. Mater. Chem. C*, 2015, **3**, 1929.
- 29 S. K. Srivastava and B. N. Avasthi, *J. Mater. Sci.* 1992, **27**, 3693.
- 30 Q. X. Gao, X. F. Wang, X. C. Wu, Y. R. Tao and J. J. Zhu, *Micro. Meso. Mater.* 2011, **143**, 333.
- 31 Q. X. Gao, X. F. Wang, Y. R. Tao and X. C. Wu, *Sci. Adv. Mater.* 2012, **4**, 327.
- 32 Y. R. Tao, X. C. Wu, W. Wang and J. N. Wang, *J. Mater. Chem. C*, 2015, **3**, 1347.
- 33 R. S. Chen, H. Y. Chen, C. Y. Lu, K. H. Chen, C. P. Chen, L. C. Chen and Y. J. Yang, *Appl. Phys. Lett.*, 2007, **91**, 223106.
- 34 J. A. Garrido, E. Monroy, I. Izpura and E. Munoz, *Semicond. Sci. Technol.* 1998, **13**, 563.
- 35 X. Xie, S. Y. Kwok, Z. Z. Lu, Y. K. Liu, Y. L. Cao, L. B. Luo, J. A. Zapien, I. Bello, C. S. Lee, S. T. Lee and W. J. Zhang, *Nanoscale*, 2012, **4**, 2914.
- 36 G. Yu, B. Lianf, H. T. Huang, G. Chen, Z. Liu, D. Chen and G. Z. Shen, *Nanotechnol.* 2013, **24**, 095703.
- 37 Z. Y. Yin, H. Li, H. Li, L. Jiang, Y. M. Shi, Y. H. Sun, G. Lu, Q. Zhang, X. D. Chen and H. Zhang, *ACS Nano*, 2012, **6**, 74.
- 38 D. Xiang, C. Han, J. L. Zhang and W. Chen, *Sci. Rep.*, 2014, **4**, 4891.
- 39 P. A. Hu, L. F. Wang, M. Yoon, J. Zhang, W. Feng, X. N. Wang, Z. Z. Wen, J. C. Idrobo, Y. Miyamoto, D. B. Geohegan and K. Xiao, *Nano Lett.*, 2013, **13**, 1649.
- 40 V. N. Sigaev, N. V. Golubev, E. S. Ignat'eva, A. Paleari and R. Lorenzi, *Nanoscale*, 2014, **6**, 1763.
- 41 Y. Teng, L. X. Song, A. Ponchel, Z. K. Yang and J. Xia, *Adv. Mater.*, 2014, **26**, 6238.